Title

MECHANISMS FOR ELECTRONIC ENERGY TRANSFER BETWEEN MOLECULES AND METAL SURFACES: A COMPARISON OF SILVER AND NICKEL

Authors

Whitmore, P.M.
Roberta, H.J.
Harris, C.B.

Publication Date

1982-03-01

LBL-13780
Preprint
UC 4

Lawrence Berkeley Laboratory
UNIVERSITY OF CALIFORNIA

Materials & Molecular Research Division

Submitted to the Journal of Chemical Physics

MECHANISMS FOR ELECTRONIC ENERGY TRANSFER BETWEEN MOLECULES AND METAL SURFACES: A COMPARISON OF SILVER AND NICKEL

P.M. Whitmore, H.J. Robota, and C.B. Harris

March 1982

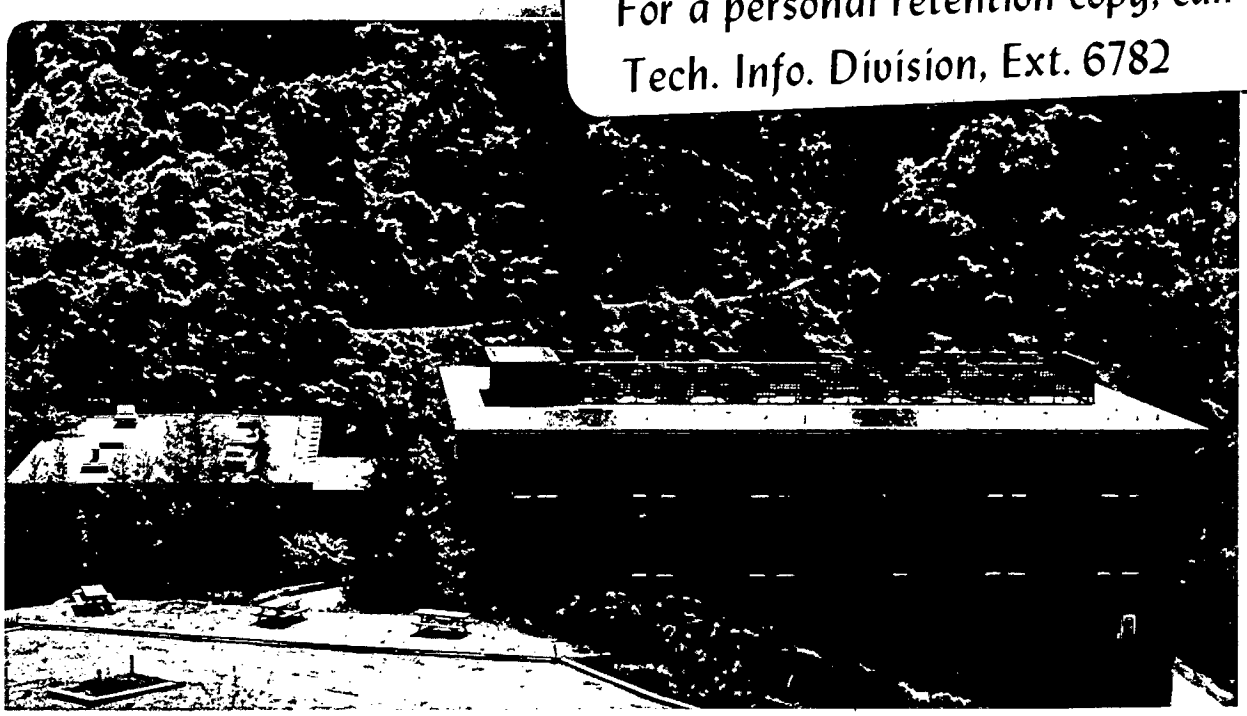

Prepared for the U.S. Department of Energy under Contract DE-AC03-76SF00098

DISCLAIMER

Mechanisms for Electronic Energy Transfer Between Molecules and Metal Surfaces: A Comparison of Silver and Nickel

P.M. Whitmore, H.J. Robota, and C.B. Harris

Department of Chemistry and Materials and Molecular Research Division of Lawrence Berkeley Laboratory,

University of California

Berkeley, California 94720

ABSTRACT

The phosphorescence lifetime of pyrazine above a Ag(111) surface has been measured as a function of molecule-metal separation between 10Å and 420Å. The distance dependence of the lifetime is in accord with the predictions of the classical point dipole theory over this range of distances. Using this classical model, the decay of electronically excited pyrazine is separated into contributions from radiative decay, resonant surface plasmon excitation, and lossy surface wave damping. The relative importance of these decay channels is calculated for silver and nickel in the near-ultraviolet, and the dominant mechanism for energy transfer to these two metals in this distance regime is interpreted in terms of the electronic structure of the metal.

This work was supported by the Director, Office of Energy Research, Office of Basic Energy Sciences, Chemical Sciences Division of the U.S. Department of Energy under Contract Number DE-AC03-76SF00098.

INTRODUCTION

A proper description of the ways in which internal excitation energy is transferred between molecules and surfaces through electromagnetic field interactions, particularly in the short distance regime, is crucial to the understanding of a wide variety of molecule-surface interactions. For energy transfer processes which occur over very short distances (on the order of atomic dimensions), a complete description necessitates a quantum mechanical approach. However, because of the large number of atoms which must be included to properly treat the surface response, this method is extremely cumbersome and not generally useful. It has been demonstrated, though, that an approximate, classical treatment can quantitatively describe the energy transfer over a large range of molecule-surface separations. The simplicity of this classical model and the physical insight it provides into the mechanisms of the energy transfer make it attractive for use in many classes of problems. Thus it becomes very important to determine in each case the distance regime over which this simple model can be used to describe the energy transfer.

In this paper, we will specifically address the validity of a classical point dipole model for the transfer of energy between an electronically excited molecule and a metal surface. Although we restrict our discussion to this particular interaction, it is important to note that the nature of the problem and the physical picture of the interaction are quite general. The application of this general classical treatment to other surface phenomena, such as vibrational energy transfer to metals or semiconductors, magnetic dipole-surface interactions, and selective surface photochemistry, may provide insight into the development of new experimental techniques for probing these processes.

There are several mechanisms through which an electronically excited molecule, viewed as an oscillating dipole, can be influenced by the proximity of a metal surface. For molecules located far from the surface (on the order of the wavelength of the dipole emission), the excited molecule will be perturbed by the radiation field reflected from the metal. This "image effect" causes the excited state lifetime to decrease, if the reflected field is out of phase with the oscillating dipole, or increase if it is in phase. At smaller molecule-metal separations, additional mechanisms become important. Collective excitations in the metal (if any), such as bulk and surface plasmons, and electron-hole pair excitations, can act as energy acceptors, provided that energy and momentum can both be conserved. The excited molecule can also begin to transfer energy through the near field components of its dipole field to the electron gas of the metal, which, through various scattering processes, can dissipate the energy into the bulk. This "lossy surface wave" mechanism is very efficient and can shorten the lifetime of an excited molecule by several orders of magnitude.

The most successful general theory of energy transfer to metal surfaces is the classical, macroscopic approach developed by Chance, Prock, and Silbey (CPS).[1] This treatment explores both the role of the metal dissipative modes and the dependence of the energy transfer rate on the metal-molecule separation. The model treats the excited molecule as a point dipole located above a metal of (local) dielectric constant $\tilde{\varepsilon}(\omega)$, which is separated from a dielectric ambient at an infinitely sharp boundary. Within this framework, the total decay rate of the excited molecule can be separated into radiative and non-radiative components, the latter representing the rate of energy transfer to the metal.

Experiments on a wide variety of systems have explored the range of

applicability of the CPS treatment by measuring the distance dependence of the energy transfer rate.[2-8] Almost all have found at least qualitative agreement with the predictions of the CPS theory, even for molecule-metal separations as small as 7Å. In those experiments which could not be explained satisfactorily by the CPS model, the investigators were unable to conclude that the approximations in the theory (e.g., point dipoles, geometrical boundary conditions, local dielectric constants) had become invalid.[6]

However, at some point a more exact treatment must be required to quantitatively describe the energy transfer process. The delocalized nature of the metal electronic states necessitates a theory which includes non-local dielectric behavior and the finite spatial extent of the molecular dipole. Further, a correct description of the metal surface region must reflect the smoothly varying electron density across the surface. Recently, theories have been developed incorporating some of these details, and deviations from the CPS behavior are predicted for distances below 7Å.[9-11]

Attempts to observe deviations from the CPS predictions, and interest in resonant energy acceptors in the metal surface, have led experimenters to systems in which energy transfer to surface plasmons is important. In particular, silver has been investigated extensively because surface plasmons are available at visible and near-UV wavelengths. Results of studies performed under relatively low vacuum conditions (2×10^{-7} torr) for the pyrazine/argon/polycrystalline evaporated silver system, in which the pyrazine $^3n\pi^*$ excited state (located at 3.3eV) occurs near the silver surface plasmon resonance (at 3.6eV), indicate that the energy transfer rate remains approximately constant for separations from 125Å down to 10Å.[6] This is in direct disagreement with the predictions of CPS theory for this system at these separations. Recently we have reported the results of our study of the

energy transfer from $^3n\pi^*$ pyrazine to a single crystal silver(111) surface in ultrahigh vacuum.[8] We found that the $^3n\pi^*$ pyrazine lifetime decreased monotonically with decreasing molecule-metal separation, and the distance dependence of the energy transfer process down to 10Å can be described quantitatively within the CPS framework. Even more recently, the experiment on evaporated silver films was repeated under better vacuum conditions and under more controlled gas depositions, and no saturation of the energy transfer rate was observed down to 35Å of the surface.[7]

In this paper, we elaborate upon our previously reported experimental work on the pyrazine/argon/silver(111) system. Having demonstrated the validity of the CPS treatment down to 10Å separation, we use this model to explore the details of the mechanism of energy transfer to silver in the near-ultraviolet. Specifically, we investigate the role of the silver surface plasmons in the quenching of molecular excited states.

EXPERIMENTAL

The experimental apparatus is shown schematically in Fig.1. Details of the configuration and capabilities of the ultrahigh vacuum chamber have been described elsewhere.[12] Typical operating pressures were $\sim 2 \times 10^{-10}$ torr. Silver samples were spark-cut from a 3/8" rod (Aremco Products, 99.999% purity), oriented to within 1° of the (111) direction by Laue backscattering, and mechanically and chemically polished. At the start of each experiment, the silver sample was cleaned by argon ion bombardment and annealing, then placed on a liquid helium cold tip which was pre-cooled to minimize condensation of residual gases on the silver surface.

The argon and pyrazine layers were constructed by condensation on the silver surface held at 20K. Thicknesses were measured with a rotating analyzer ellipsometer which has been previously described.[12] The ellipsometric parameters (Δ,ψ) were measured continually during depositions at λ=3000Å. The refractive index of the argon layer was determined by the method of Malin and Vedam[13] and is illustrated in Fig.2. Each curve represents the set of complex refractive indices (n,k) which, for a purely real overlayer thickness, will reproduce the (Δ,ψ) values measured at one point during the deposition. The intersection of these curves is then the actual refractive index the argon layer. The result of this determination, $\tilde{n}(Ar)=1.2-.03i$, remained approximately constant throughout these experiments. This refractive index of argon was used to calculate the thicknesses of the spacer layers, with errors which we estimate to be 5-10% for all but the thinnest spacers (for which the error was probably about 5Å, the thickness of one argon layer). A monolayer of pyrazine was condensed on top of the argon spacer.

The pyrazine emission was excited at 3250Å by a linearly polarized 10

nsec pulse from the frequency-doubled output of a Nd:YAG pumped dye laser (Quanta-Ray Corp.) operating with DCM dye. The phosphorescence was collected with a one-inch f/1 lens mounted inside the vacuum chamber. Outside the chamber, the emission was isolated with colored glass filters (Schott GG375 and Corning CS7-54) and focussed onto the photocathode of a photomultiplier (EMI 6256S). The phosphorescence decay was recorded with a transient waveform digitizer (Biomation 8100) interfaced to a laboratory microcomputer (Digital Equipment Corp. PDP11/03) for signal averaging and storage on floppy disks. Phosphorescence lifetimes were calculated with a least squares fit of a single exponential to the experimental decay.

RESULTS

Phosphorescence decays were recorded for pyrazine-silver separations between 420Å and 10Å. The 10Å distance represents only two layers of argon separating the pyrazine from the silver surface. For fixed incident laser power, the phosphorescence intensity decreased with decreasing distance to the silver surface. Attempts to measure phosphorescence from pyrazine on a single monolayer of argon (5Å from the Ag surface) failed due to extremely low signal levels. The phosphorescence decays were recorded for laser excitation polarized both in and perpendicular to the plane of incidence, and, to within experimental error, the results for the two polarizations were identical. (Although the fact that the phosphorescence lifetimes were identical for both laser polarizations could be evidence for all the pyrazine molecules being oriented perpendicular to or parallel to the silver surface, we believe it more probable that we have a distribution of molecular orientations with respect to the surface. We then detect predominantly the dipoles parallel to the surface because at these distances their radiative probability is 2-20 times greater than that of perpendicular dipoles[6]).

Phosphorescence lifetimes were calculated by fitting the decays to a single exponential, and the results are presented in Table 1. For all separations studied, the fit of a single exponential to the measured decay was excellent, although there is some evidence for more rapid decay at very short times following excitation (see Fig.3). We believe that this short lifetime component is due to phosphorescence from pyrazine adsorbed near a small number of surface defects.

The observed distance dependence of the pyrazine phosphorescence lifetime was compared to the behavior predicted by the CPS theory. The model used corresponded to our experimental configuration: a layer of pyrazine 3Å above an argon layer adsorbed on a silver surface. The ambient was vacuum ($\tilde{\varepsilon}$=1), and the optical constants of the Ag and Ar at 3800Å were measured ellipsometrically during the experiment ($\tilde{\varepsilon}$(Ag)=-3.6+.15i at 3800Å). The emission wavelength of pyrazine was 3800Å, and a value of 0.3 for Φ_P, the phosphorescence quantum yield, was taken from the literature.[14] The only adjustable parameter was τ_0, the phosphorescence lifetime of pyrazine at an argon/vacuum interface at infinite separation from the silver surface.

The total decay rate for dipoles oriented parallel to the silver surface was calculated from the equations in Ref.15:

$$\frac{b}{b_0} = \frac{\tau_0}{\tau} = 1 + \frac{3}{4}\Phi_P \, \mathrm{Im} \int_0^\infty \left[\left(\frac{1-u^2}{u^2}\right)\mathcal{R}^{\parallel} + \frac{1}{u^2}\mathcal{R}^{\perp}\right] e^{-2l_1\hat{d}_1} \frac{u^3}{l_1} \, du \qquad (1)$$

where the explicit formulas for the reflectivities $\mathcal{R}$ and normalized distance $\hat{d}_l$ may be found in Ref.15, equations 2-5. Details of the derivation of this formula are to be found in Ref.1. Only the calculation for the parallel dipole is shown because, as noted previously, in this distance regime the

probability for radiative decay of parallel dipoles is much greater than that of perpendicular dipoles.

Figure 4 shows the result of the calculation for τ_0=25 msec, plotted with the experimentally determined lifetimes. The value of 25 msec for τ_0 is comparable to the phosphorescence lifetime of pyrazine in a variety of environments.[6,16] Excellent agreement is found between the observed distance dependence of the lifetime and the prediction of the CPS theory.

DISCUSSION

A detailed analysis of the CPS description can provide insight into the fundamental nature of the energy transfer process. Following Chance, et al.[1], an oscillating dipole near a surface is driven by its own electric field which has been reflected from the interface. The equation of motion for the dipole is:

$$\ddot{\mu} + b_0\dot{\mu} + \omega^2\mu = \frac{e^2}{m} E_R \qquad (2)$$

where ω is the natural oscillation frequency of the undamped dipole, b_0 is the decay rate for the dipole in the absence of a reflecting surface, m is the effective mass of the dipole, and E_R is the reflected electric field at the dipole position. The reflected field will clearly oscillate with the same frequency and lifetime as the driven dipole. If one then assumes a functional form

$$\mu = \mu_0 e^{-i(\omega + \Delta\omega)t} e^{-bt/2} \qquad (3)$$

$$E_R = E_0 e^{-i(\omega + \Delta\omega)t} e^{-bt/2} \qquad (4)$$

and substitutes into the equation of motion, the frequency shift $\Delta\omega$ and new decay rate b can be calculated. For the cases of interest here, the frequency shift is negligibly small. In terms of the classical expression for the quantum yield ($q=b_r/b$), the normalized decay rate is found to be

$$\hat{b} = \frac{b}{b_0} = 1 + \frac{3q\tilde{\varepsilon}_1}{2\mu_0 k_1^3} \mathrm{Im}(E_0) \qquad (5)$$

where $\tilde{\varepsilon}_1$ is the dielectric constant of the medium in which the dipole is imbedded, and k_1 is the propagation constant in that medium ($k_1 = \omega \tilde{\varepsilon}_1^{1/2}/c$). The calculation of the decay rate of the dipole in the presence of the surface thus becomes a problem of determining the reflected field at the dipole.

The calculation of the electric field at a dipole near an interface has been treated by a number of authors.[1,9-11,17-20] Chance, et al.[1], followed the derivation of Sommerfeld.[17] The details of the calculation depend upon the geometry of the dielectric interfaces and dipole orientation, and thus only the general procedure for the solution will be described here. Sommerfeld's treatment calculates the electric field from the Hertz vectors associated with the dipole (i.e., the electrodynamic vector potentials). In order to describe the spatial variation of the field, the dipole field is Fourier analyzed in terms of different wave vector components. In other words, the Hertz vectors are constructed as a superposition of eigenfunctions (with associated eigenvalues u, the normalized wave vector) which will reproduce the spatial variation of the dipole field. Once this superposition has been created, the effect of the reflecting surface on the dipole field can be included by matching the Maxwell boundary conditions for each Fourier (wave

vector) component at the interface. The electric field can then be evaluated at the position of the dipole.

The general result for the reflected electric field at the dipole is an integral over all wave vector components of the form:

$$E_R = \int_0^\infty [B\mathcal{R}'' + C\mathcal{R}^\perp]\ e^{-2l_1\hat{d}_1}\ \frac{u^3}{l_1}\ du \qquad (6)$$

where $\mathcal{R}$ is the complex Fresnel reflection coefficient, $\hat{d}_1$ is the (normalized) distance from the dipole to the surface, and $l_1 = -i(1-u^2)^{1/2}$. The coefficients B and C are determined from the geometry and dipole orientation in a specific case. The term in brackets represents the amplitude change (contained in the appropriate reflection coefficients) and the exponential is the phase change for each wave vector component of the electric field after reflection back to the dipole. Inserting this form for the reflected field into the expression for the decay rate yields:

$$\hat{b} = 1 + Aq\ \mathrm{Im} \int_0^\infty [B\mathcal{R}'' + C\mathcal{R}^\perp]\ e^{-2l_1\hat{d}_1}\ \frac{u^3}{l_1}\ du \qquad (7)$$

where q is the free molecule quantum yield, and the coefficients A, B, and C for various special cases have been evaluated in Refs. 1 and 15. The values of A, B, and C appropriate to our experimental geometry were used to calculate the theoretical decay rate from the numerical solution of equation 1 (see Results section).

The second term of equation (7) thus describes the modification of the total decay rate of an excited dipole due to its proximity to a surface. The imaginary part of the integrand describes the coupling of the various wave vector components of the dipole field to the decay channels available. As noted previously,[1] the integral over all wave vector components in equation (7) can be separated into contributions corresponding to the different decay mechanisms. This separation can easily be rationalized in terms of a physical picture of the interaction of the dipole field with a surface. Fig.5a shows the radiation field associated with a dipole at one instant during its oscillation. The dipole field induces a surface charge on the metal, and the dipoles associated with this oscillating surface current set up their own radiation field pattern (not shown on Fig.5a). The interference of this reflected radiation field with the directly emitted dipole radiation leads to the modulation of the radiative decay rate at large distances, described by Drexhage.[21] It is clear from the radiation field pattern in Fig.5a that those surface dipoles with wavelength larger than the dipole emission wavelength (i.e., with wave vector smaller than the photon wave vector) will participate in modifying the decay rate of the dipole through its radiation field. Thus, the integral of equation (7) over normalized wave vector $0<u<1$ represents this modification of the radiative decay rate of the dipole.[1]

The energy transfer to the metal surface, however, takes place through the "static" and "induction" field of the dipole. Fig.5b shows (on a much smaller scale than Fig.5a) the near field of a dipole at one instant during its oscillation. The electric field of the dipole again induces a surface charge separation, but here the associated surface dipoles all have wavelengths less than that of the radiation field pattern. Thus, these dipole field components which will dissipate energy into the metal through some loss

mechanism all have wave vectors greater than the photon wave vector. The integral in equation (7) from $1<u<\infty$ represents this total energy transfer rate into the metal. Also shown in Fig.5b is the oscillating surface dipole whose wave vector exactly matches the surface plasmon wave vector at this energy. This dipole field component can thus transfer energy by exciting this surface charge oscillation, which can propagate far from the dipole position before decaying into bulk excitations (see below).

A close examination of this energy transfer rate for the specific case of pyrazine on silver provides valuable insight into the mechanisms for the transfer process. Figures 6a and 6b plot the imaginary part of the integrand of equation (1) as a function of the normalized wave vector u for various pyrazine-silver separations. The area under these curves is proportional to the energy transfer rate from $^3n\pi^*$ pyrazine to the silver surface.

Although a rigorous separation of the energy transfer rate into different mechanisms has not been achieved theoretically, the occurrence of two prominent features in Fig.6 makes such a separation attractive. Each curve displays a large, narrow peak near u=1.3, and for pyrazine-silver separations less than 200Å a broad feature at higher wave vector develops, growing in intensity and shifting to larger wave vector as the separation decreases.

The sharp peak at u=1.3 is attributed to energy transfer via excitation of resonant surface plasmons on silver. The (normalized) wave vector for surface plasmons on silver at 3.3eV (the dipole emission energy) is $u_{sp}=1.3$. Thus, the wave vector components of the dipole field at u=1.3 can match both energy and momentum (wave vector) with the silver surface plasmon, and resonant energy transfer takes place. This plasmon excitation occurs over rather large distances (several hundred Å), and appears to be important over a wide range of metal-molecule separations.

At shorter separations (less than 200 Å), the energy transfer through higher wave vector components becomes significant. This decay proceeds via "lossy surface waves"; that is, the driving of nearly free electrons in the surface which then dissipate energy through scattering processes in the metal. Although such scattering processes in silver are not very efficient at this energy ($Im(\tilde{\varepsilon})=.15$ at $\lambda=3800$Å), the proximity of a surface plasmon resonance at $\lambda=3540$Å guarantees a large number of (non-resonant) surface plasmons acting as mediators for the energy transfer to the bulk. As demonstrated before,[1] the rate of energy transfer via these lossy surface waves, which becomes important for dipoles close to the surface, varies as the cube of the dipole-surface separation.

The expression for the total decay rate (equation 1) can now be separated into three parts (following Weber and Eagen[22]), representing the decay of the dipole through: 1) emission of photons; 2) resonant excitation of surface plasmons; 3) energy transfer to the metal through the driving of lossy surface waves. The relative importance of each of these decay channels is illustrated in Fig.7, which is a plot of the probability for decay of the excited molecule through each path as a function of dipole-metal separation. At very large distances, the decay of the excited dipole via photon emission is the most probable of the three mechanisms. As the dipole approaches the surface, resonant excitation of surface plasmons begins to compete with photon emission until, at 100Å-500Å separation, energy transfer through surface plasmon excitation is the predominant mode of decay. Below about 100Å, nonradiative energy transfer to the metal via lossy surface waves dominates all other decay channels. The probabilities for photon emission and surface plasmon excitation become extremely small at short separations due to competition with the lossy wave mechanism, and as a result our attempts to detect

phosphorescence from pyrazine below 10Å were unsuccessful. At separations shorter than 100Å, then, where energy transfer through lossy waves dominates, the energy transfer rate should exhibit a cubic distance dependence. Fig.8 shows on a logarithm plot that the measured decay rate does in fact vary as d^3 below 100Å.

The importance of surface plasmon excitation in the energy transfer process on silver can be illustrated by a comparison with the energy transfer from $^3n\pi^*$ pyrazine to nickel. In an earlier experiment,[2] the energy transfer rate for the pyrazine/argon/nickel(111) system was shown to exhibit a cubic distance dependence from 7Å to (at least) 100Å. On nickel, the energy of the excited pyrazine molecule (3.3 eV) is located far from the surface plasmon resonance (8.1 eV), so the number of surface plasmons near 3.3 eV should be much smaller than on silver. Thus, surface plasmon excitation is expected to be much less important in the energy transfer from pyrazine to nickel at λ=3800Å. Figures 9a and 9b show the contributions to the nonradiative rate from the different (normalized) wave vector components of the dipole field. As before with silver, two different energy transfer channels are apparent: the small, sharp feature near u=1 representing resonant excitation of surface plasmons, and the large, broad contribution from lossy surface waves at higher wave vector.

The similarity of this behavior with that of silver in Figures 6a and 6b is striking, yet the differences in the magnitudes of the contributions in the two cases is significant. The resonant excitation of surface plasmons is very small in nickel, nearly 30 times smaller than in silver where the surface plasmon resonance is much nearer the pyrazine excited state energy. The energy transfer through lossy surface waves (i.e., the integrated area under the high wave vector peak) is much greater in nickel than in silver because

scattering into bulk electron-hole interband transitions is very efficient ($Im(\tilde{\epsilon})=8.53$ for nickel at $\lambda=3800$Å). The total decay rate in the case of nickel shows almost no contribution from the excitation of surface plasmons (see Fig.10) and is dominated by energy transfer through lossy waves below about 400Å separation.

An illustration of the importance of surface plasmons in the energy transfer to silver is provided in Figure 11, which plots the ratio of the energy transfer rates to silver and nickel as a function of distance for various energies. When the value of this ratio becomes greater than one, the energy transfer process is more efficient on silver than on nickel. At low energy (near 2.0 eV), energy transfer to silver is faster than to nickel only at separations around 2000Å. Transfer to surface plasmons on silver is greatest at this distance and is responsible for the larger transfer rate. As the energy increases toward the surface plasmon resonance in silver, more surface plasmons become available to silver to act as energy acceptors. The maximum of the ratio of energy transfer rates thus increases and also moves to shorter separation where the plasmon excitation probability is greatest. When the energy being transferred is almost equal to the silver surface plasmon resonance, the transfer rate is greater on silver than nickel for all distances shorter than 500Å. At this energy the silver surface has available a large number of surface plasmons to receive the excitation energy, and these plasmons are also strongly coupled to bulk scattering mechanisms which make the energy transfer very efficient. As a function of energy, the maximum of the ratio of the transfer rate seems to reflect the density of states of the surface plasmons on silver, for it is only through plasmon excitation that the energy transfer to silver becomes more rapid than the transfer to nickel.

CONCLUSION

We have measured the distance dependence of the phosphorescence lifetime of $^3\pi\pi^*$ pyrazine above a silver(111) surface between 10Å and 420Å separation. We find a monotonic decrease in the lifetime as the dipole-metal separation decreases, in quantitative agreement with the prediction of the Chance, Prock, and Silbey theory. Attempts to measure the lifetime for distances less than 10Å were unsuccessful. Analysis of the CPS model has shown that surface plasmons on silver play an important role in the energy transfer in the near-UV.

ACKNOWLEDGEMENTS

This work was supported by the Director, Office of Energy Research, Office of Basic Energy Sciences, Chemical Sciences Division of the U.S. Department of Energy under Contract No. DE-AC03-76SF00098. The authors are extremely indebted for the support of the San Francisco Laser Center, a National Science Foundation Regional Instrumentation Facility, NSF Grant No. CHE79-16250 awarded to the University of California at Berkeley in collaboration with Stanford University. The authors also wish to thank Professor H. Metiu for providing us with reports of his work prior to publication.

REFERENCES

1. R.R. Chance, A. Prock, and R. Silbey, Adv. Chem. Phys., 37, 1 (1978).

2. A. Campion, A.R. Gallo, C.B. Harris, H.J. Robota, and P.M. Whitmore, Chem. Phys. Lett.,73, 447 (1980).

3. A. Adams, R.W. Rendell, W.P. West, H.P. Broida, P.K. Hansma, and H. Metiu, Phys. Rev. B 21, 5565 (1980).

4. C.F. Eagen, W.H. Weber, S.L. McCarthy, and R.W. Terhune, Chem. Phys. Lett., 75, 274 (1980).

5. I. Pockrand, A. Brillante, and D. Mobius, Chem. Phys. Lett.69, 499 (1980).

6. R. Rossetti and L.E. Brus, J. Chem. Phys., 73, 572 (1980).

7. R. Rossetti and L.E. Brus, J. Chem. Phys., 76, 1146 (1982).

8. P.M. Whitmore, H.J. Robota, and C.B. Harris, J. Chem. Phys., 76, 740 (1982).

9. B.N.J. Persson, J. Phys. C 11, 4251 (1978).

10. G.E. Korzeniewski, T. Maniv, and H. Metiu, Chem. Phys. Lett., 73, 212 (1980).

11. G.E. Korzeniewski, T. Maniv, and H. Metiu, J. Chem. Phys., 76, 1564 (1982).

12. H.J. Robota, P.M. Whitmore, and C.B. Harris, J. Chem. Phys., 76, 1692 (1982).

13. M. Malin and K. Vedam, Surf. Sci., 56, 49 (1976).

14. S.L. Madej, G.D. Gillispie, and E.C. Lim, Chem. Phys., 32, 1 (1978).

15. R.R. Chance, A. Prock, and R. Silbey, J. Chem. Phys., 65, 2527 (1976).

16. R. Rossetti and L.E. Brus, J. Chem. Phys.,70, 4730 (1979), and references therein.

17. A. Sommerfeld, Partial Differential Equations in Physics, Academic, New York, 1949.

18. G.S. Agarwal, Phys. Rev. A 11, 230, 243, 253 (1975); Phys. Rev. A 12, 1475 (1975).

19. W. Lukosz and R.E. Kung, J. Opt. Soc. Am., 67, 1607, 1615 (1977).

20. J.E. Sipe, Surf. Sci., 105, 489 (1981).

21. K.H. Drexhage, Sci. Am., 222, 108 (1970).

22. W.H. Weber and C.F. Eagen, Optics Lett., 4, 236 (1979).

23. P.B. Johnson and R.W. Christy, Phys. Rev. B 9,5056 (1974).

24. P.B. Johnson and R.W. Christy, Phys. Rev. B 6,4370 (1972).

FIGURE CAPTIONS

Figure 1: A schematic view of the experimental apparatus and experimental geometry. 1) Single crystal Ag(111) surface; 2) Liquid helium cryostat sample mount; 3) f/1 collection lens with conical shroud; 4) External focussing lens; 5) Colored glass filters; 6) Photomultiplier tube in a dry ice cooled housing; 7) Spherical mirror for use in ellipsometry; 8) Ellipsometer MgF_2 input polarizer; 9) Ellipsometer alignment apertures; 10) Rotating analyzer polarizer, motor, and photomultiplier; 11) Excitation laser alignment apertures; 12) MgF_2 polarizer for polarizing the excitation laser.

Figure 2: A plot of the (n,k) values which, for purely real layer thicknesses, reproduce the measured (Δ,ψ) parameters at seven points during the deposition. The interaction is the actual complex refractive index of the argon spacer.

Figure 3: The logarithm of the phosphorescence intensity of $^3\pi\pi^*$ pyrazine 100Å above Ag(111) versus time. The line is the best least-squares exponential (τ=10.8 msec).

Figure 4: The lifetime of $^3\pi\pi^*$ pyrazine above Ag(111) vs. argon spacer thickness. The points are experimental values, and the solid curve is the behavior calculated from the Chance, Prock, and Silbey model (see text for details).

Figure 5: The electric field lines associated with a dipole near a metal surface at one instant during its oscillation. a) The surface charge induced by the radiation field of the dipole. The periodic charge density oscillation has wavelengths greater than that of the radiation pattern (i.e., $k<k_{photon}$). b) The surface charge induced by near field components of the dipole. Here the wavelengths of the surface dipoles are shorter than that of the radiation field ($k>k_{photon}$). The surface charge oscillation whose wavelength matches

that of the surface plasmon at this energy (λ_{SP}) will propagate away from the dipole and transfer energy from the dipole (surface plasmon excitation). The other high wave vector field components dissipate energy through coupling to bulk scattering processes.

Figure 6: The imaginary part of the integrand of equation 1 vs. normalized wave vector u showing surface plasmon contribution (at u_{SP}) and lossy wave contribution (at large u) to energy transfer from pyrazine to Ag(111) at several distances. The pyrazine layer is taken to be 3Å above the argon spacer, and $\tilde{\varepsilon}$(Ag)=-3.6+.15i and $\tilde{\varepsilon}$(Ar)=1.44 at λ=3800Å. a) 1<u<10; b) 1<u<100.

Figure 7: Calculated probability for decay of $^3n\pi^*$ pyrazine on Ag(111) into photons (RD), resonant surface plasmons (SP), and lossy waves (LW), as a function of argon spacer thickness. Geometry and optical constants same as in Fig. 6. Phosphorescence quantum yield of $^3n\pi^*$ pyrazine Φ_P=0.3.

Figure 8: Logarithm plot of normalized decay rate vs. argon thickness for $^3n\pi^*$ pyrazine above Ag(111). Points are experimental measurements, curve is calculated rate (see text for details). The energy transfer to lossy waves occurs below 100Å, where rate increases as d^3 (slope of logarithm plot=3).

Figure 9: The imaginary part of the integrand of equation 1 vs. normalized wave vector u calculated for $^3n\pi^*$ pyrazine 3Å above argon spacers of various thicknesses on nickel. Optical constants for nickel at λ=3800Å were taken from Ref. 23. $\tilde{\varepsilon}$(Ar)=1.44. a) 1<u<10; b) 1<u<100.

Figure 10: Calculated probability of decay of $^3n\pi^*$ pyrazine on nickel into photons (RD), resonant surface plasmons (SP), and lossy waves (LW), as a function of argon spacer thickness. Geometry and constants same as in Fig. 9. Φ_P=0.3 taken from Ref. 14.

Figure 11: Calculated ratio of energy transfer rates to silver and to nickel as a function of distance for different energies. Values of optical constants

taken from Ref.23 and Ref.24.

Table 1: Lifetime of $^3n\pi^*$ pyrazine on argon over Ag(111).

d (Å)	τ(msec)
10	.2
20	.5
25	.5
35	1.5
50	4.0-4.9
75	3.9-8.9
100	10.1-11.8
180	14.2
420	16.0

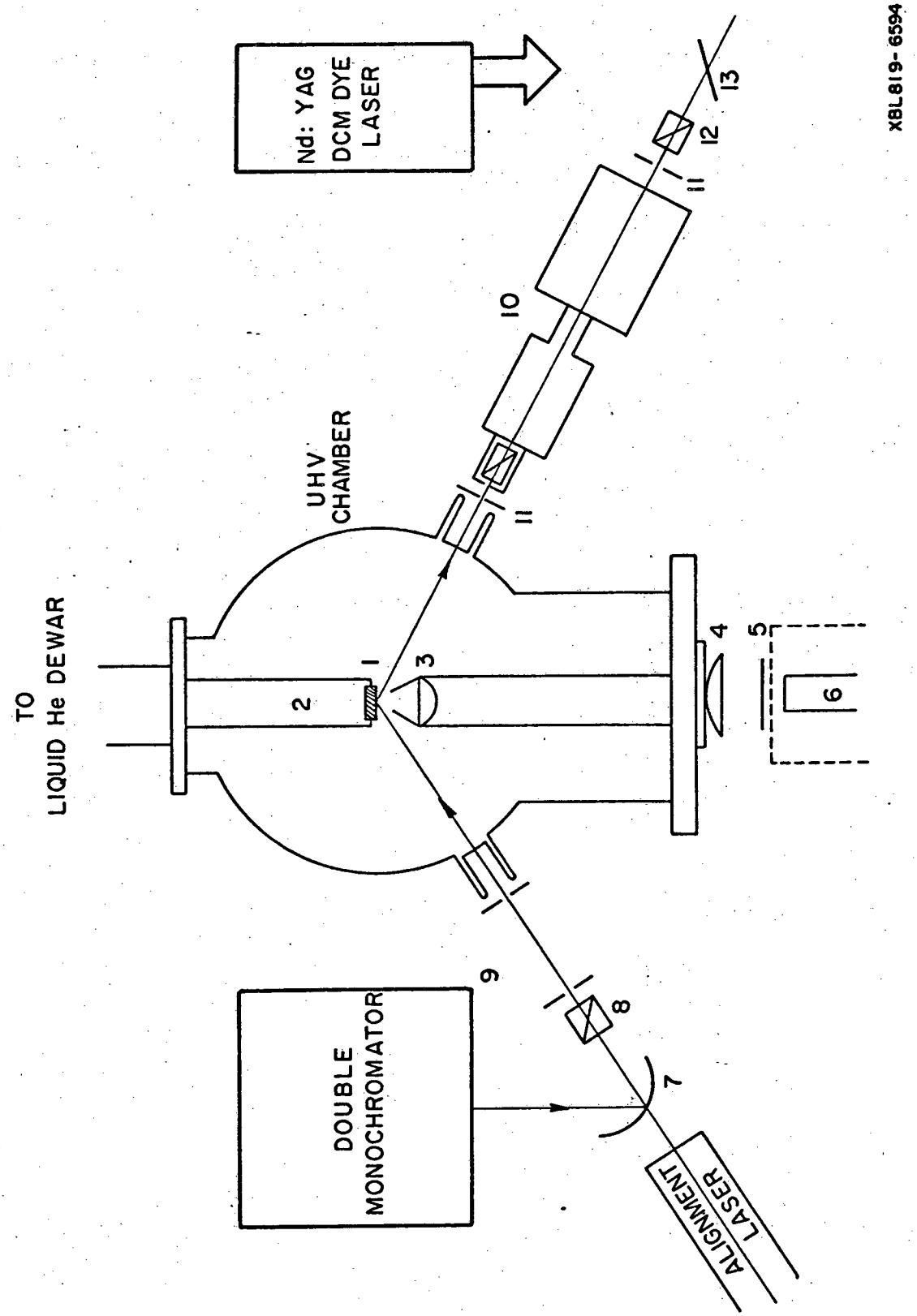
Nd: YAG
DCM DYE
LASER
UHV
CHAMBER
TO
LIQUID He DEWAR
DOUBLE
MONOCHROMATOR
ALIGNMENT
LASER
1
2
3
4
5
6
7
8
9
10
11
12
13
XBL819-6594

Figure 1

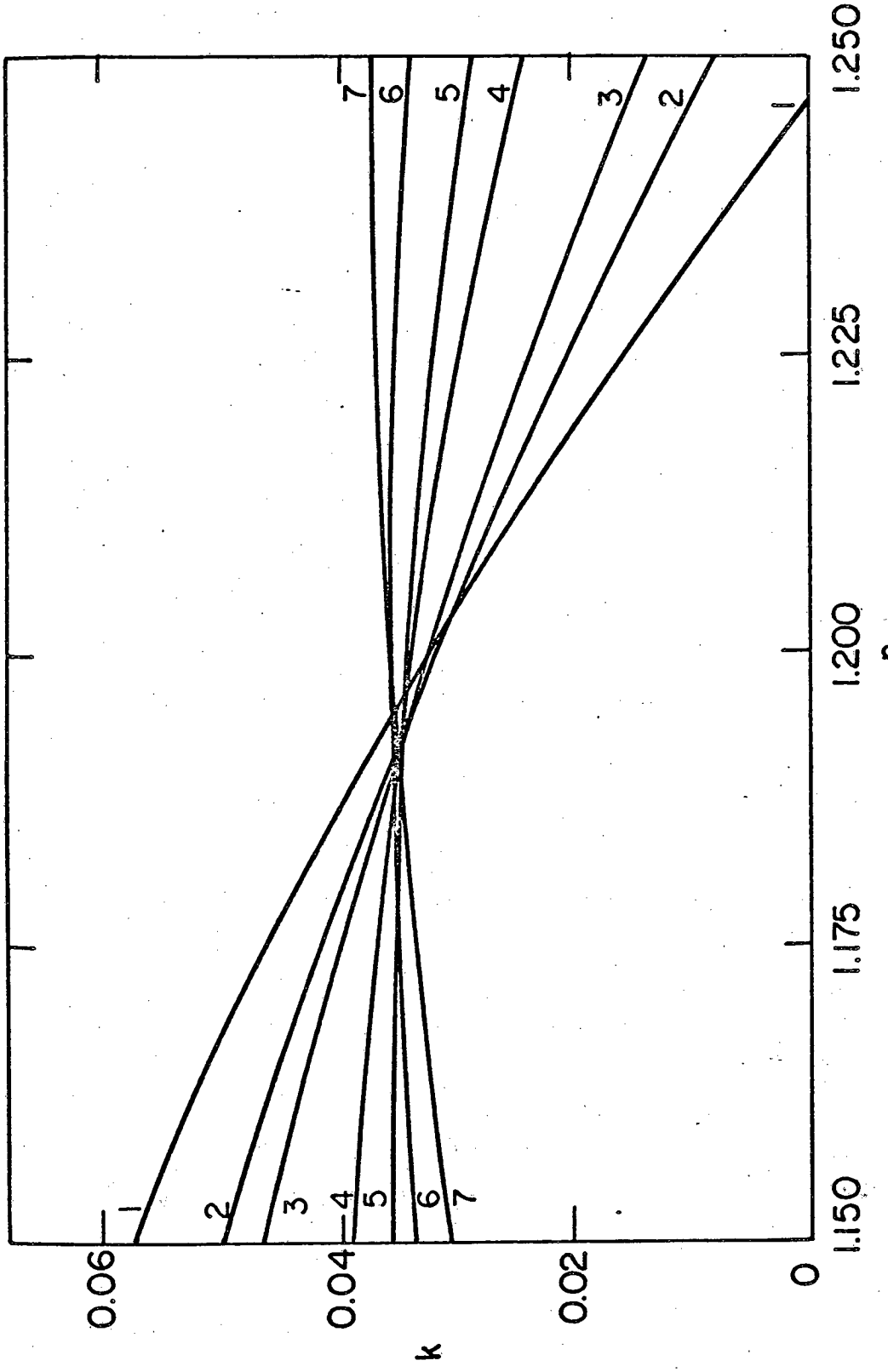

XBL 819-6587

Figure 2

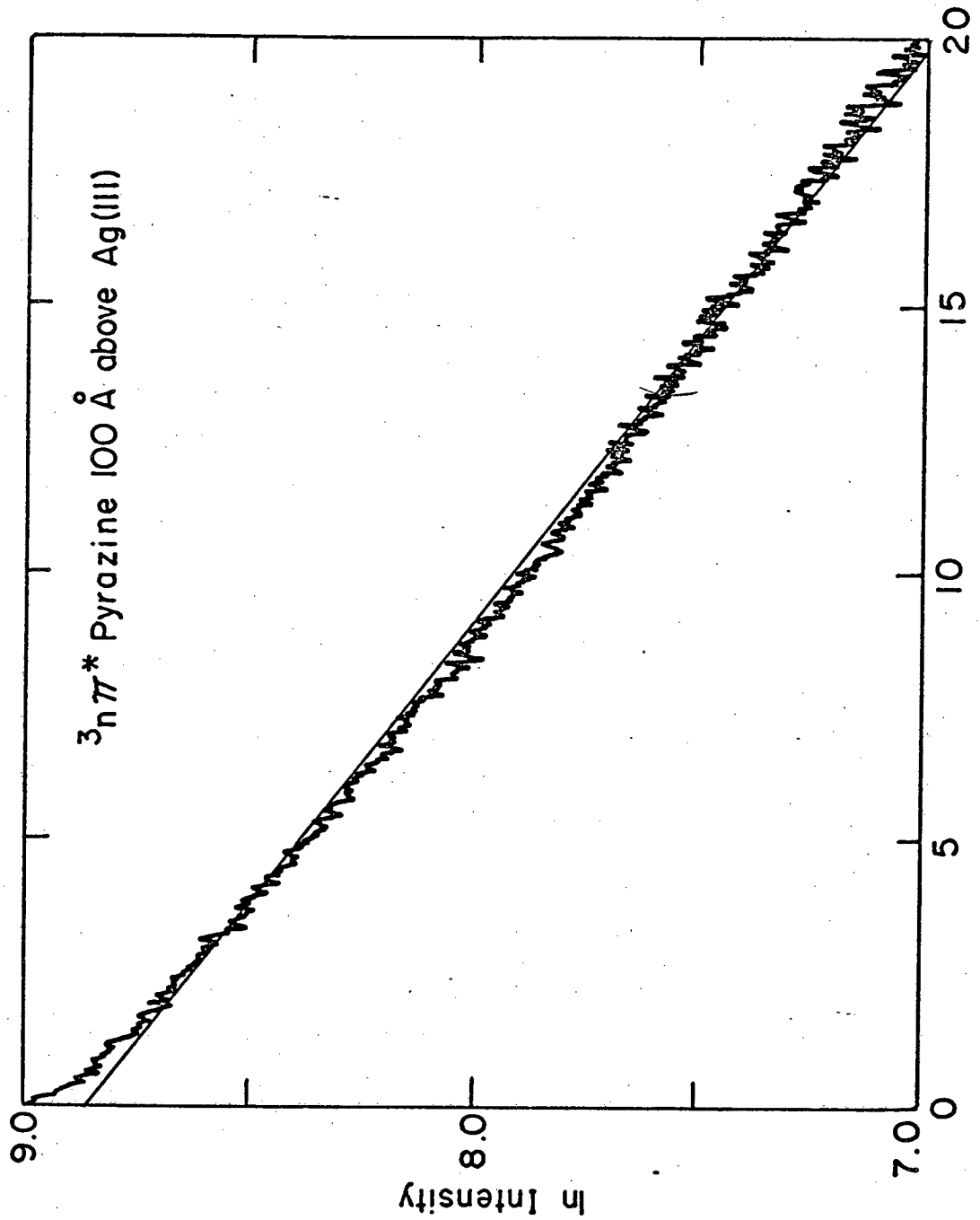
$^3n\pi^*$ Pyrazine 100 Å above Ag(111)
ln Intensity
9.0
8.0
7.0
0
5
10
15
20
Time (msec)
XBL 819 - 6589

Figure 3

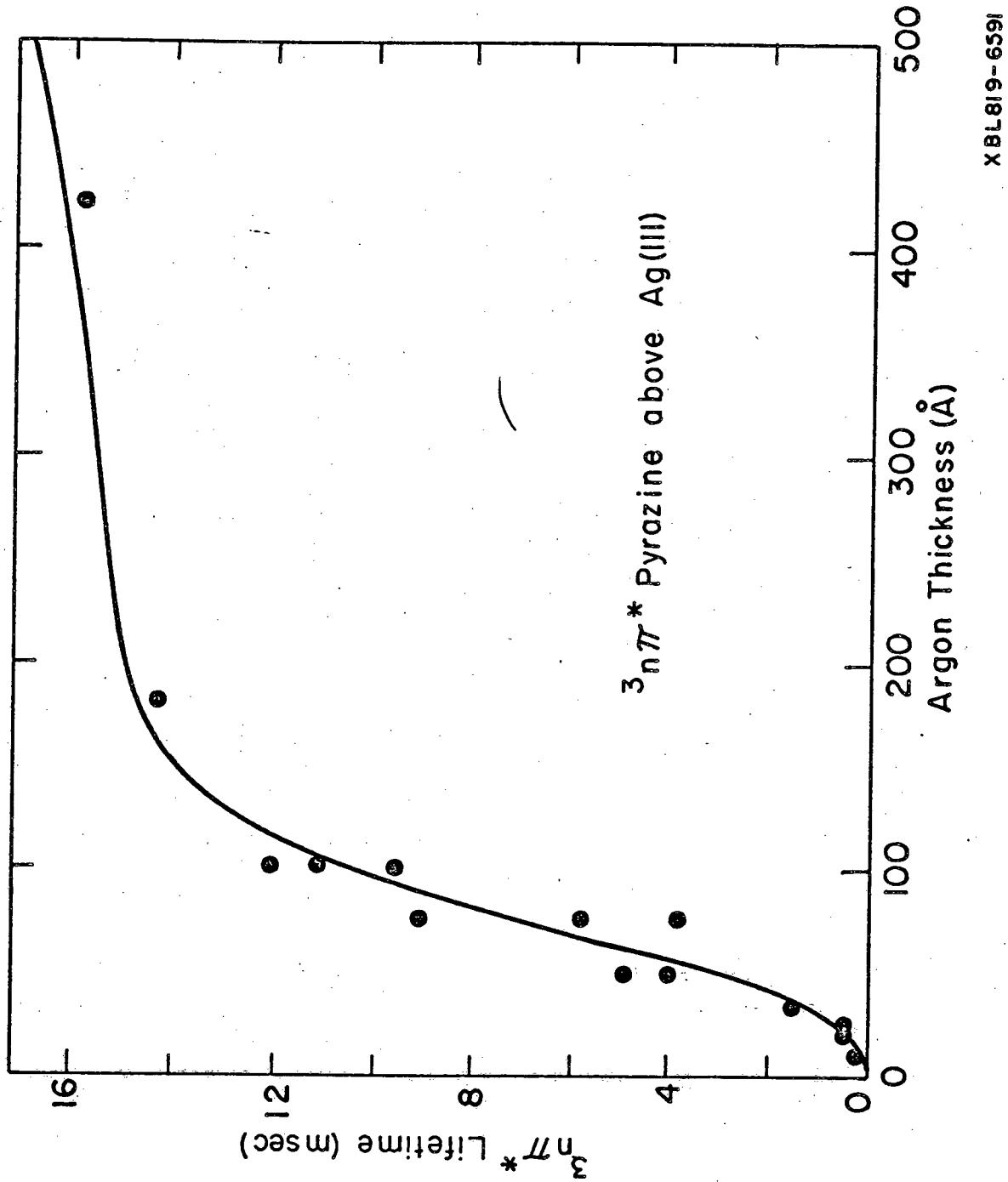
$^3n\pi^*$ Lifetime (msec)
0
4
8
12
16
0
100
200
300
400
500
Argon Thickness (Å)
$^3n\pi^*$ Pyrazine above Ag(111)
XBL819-6591

Figure 4

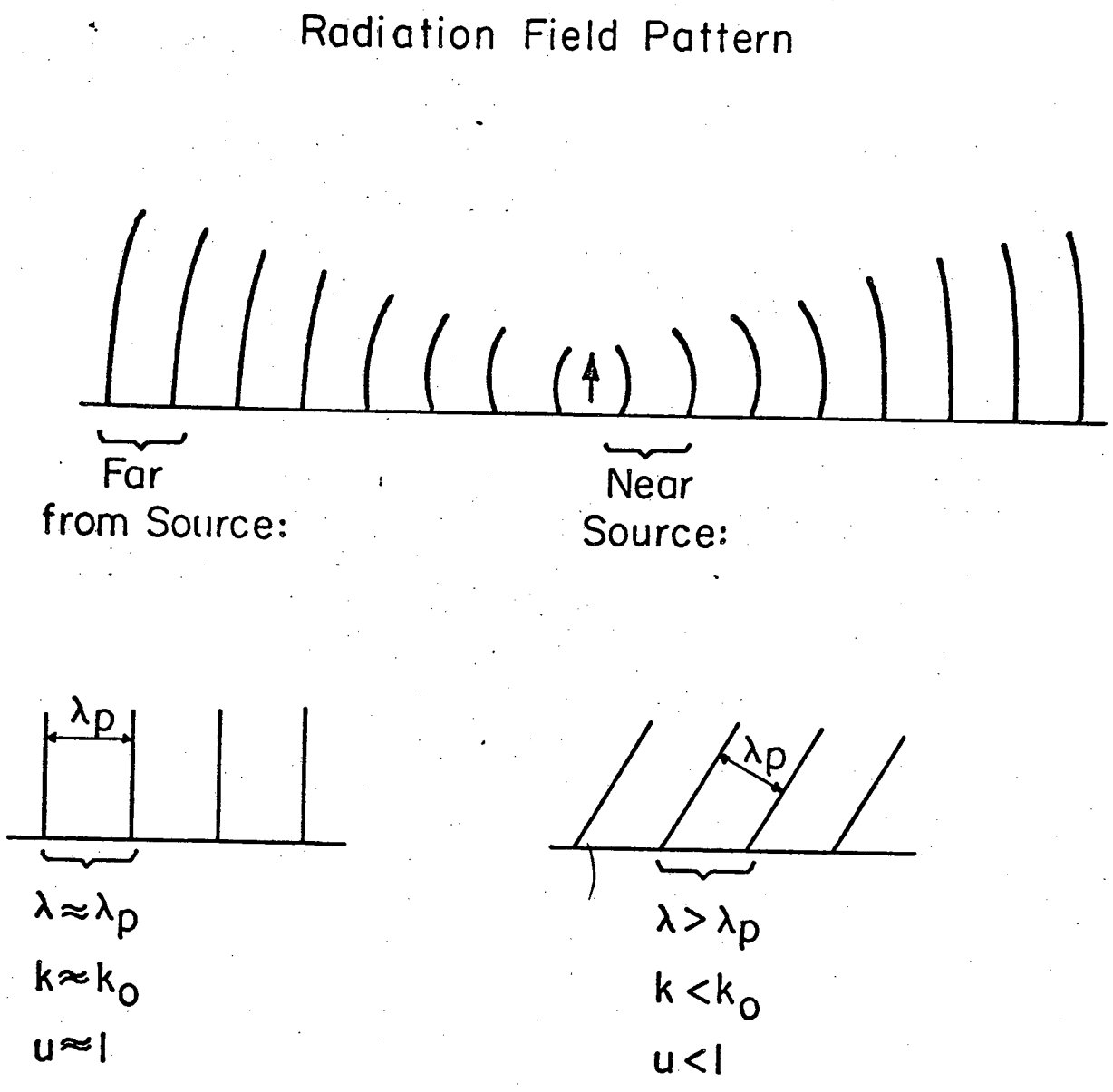
Radiation Field Pattern
Far
from Source:
Near
Source:
λp
λp
λ≈λp
k≈k0
u≈1
λ>λp
k<k0
u<1
XBL 821-5064

Figure 5a

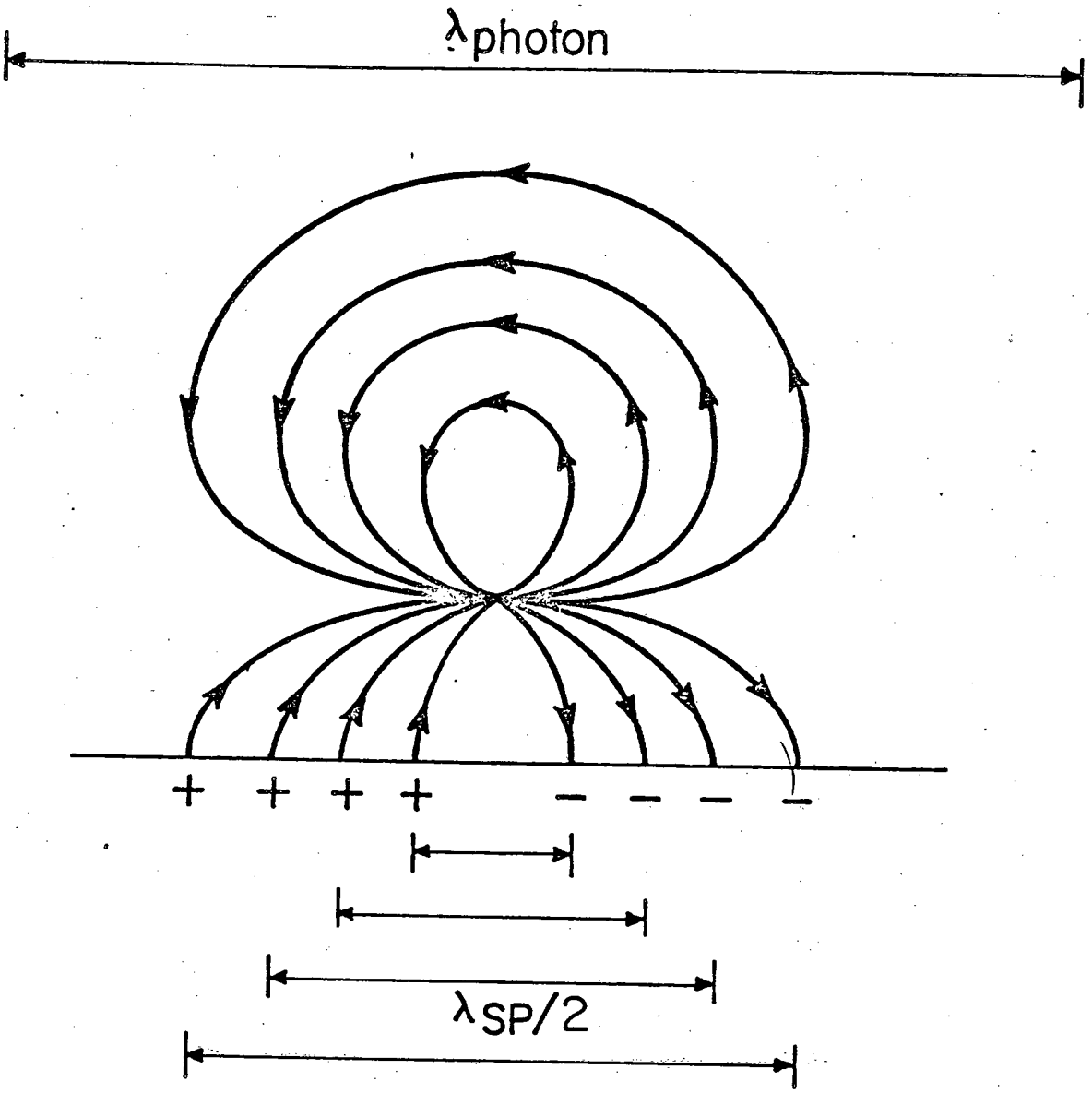

XBL821-5000

Figure 5b

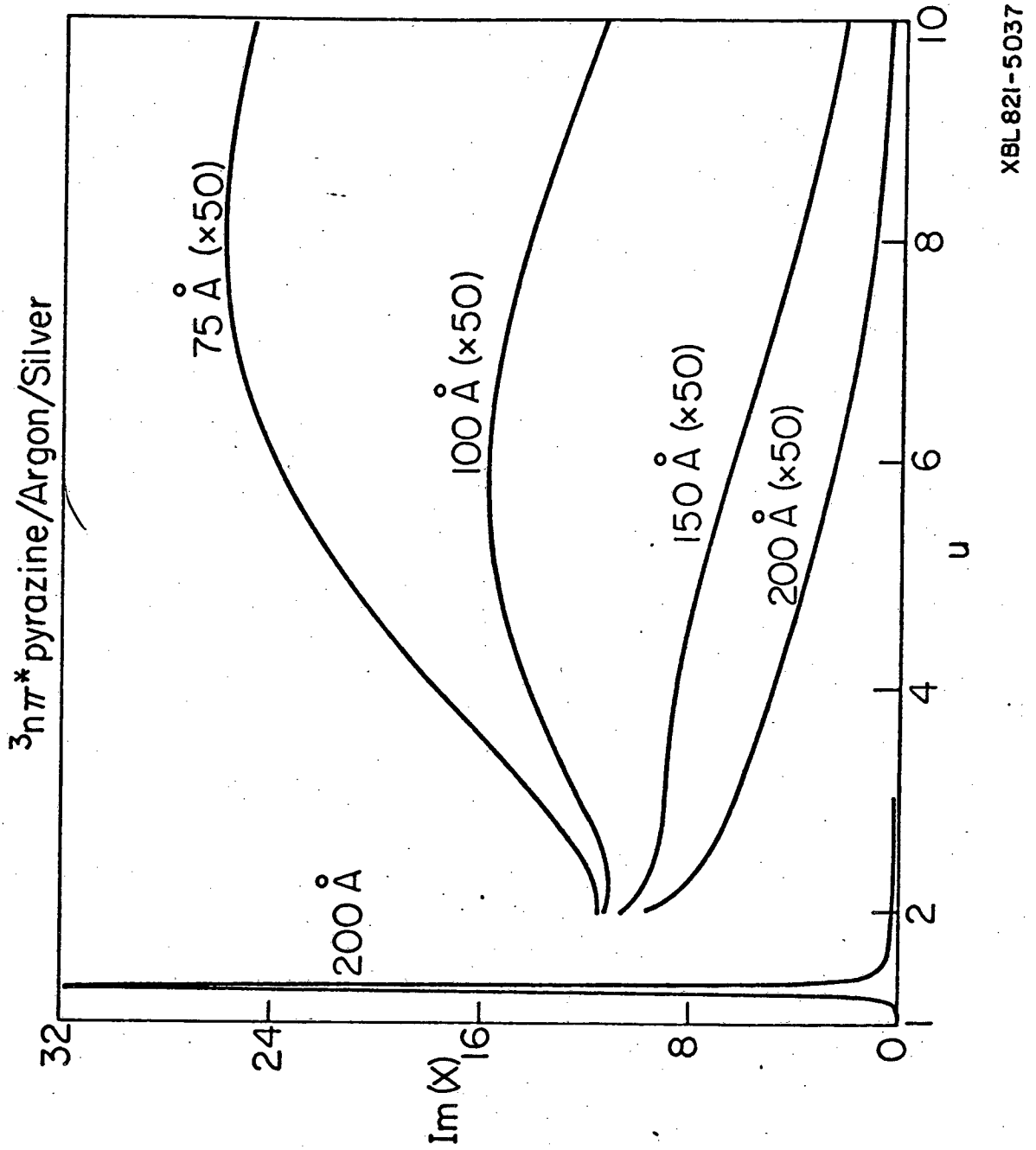

XBL821-5037

Figure 6a

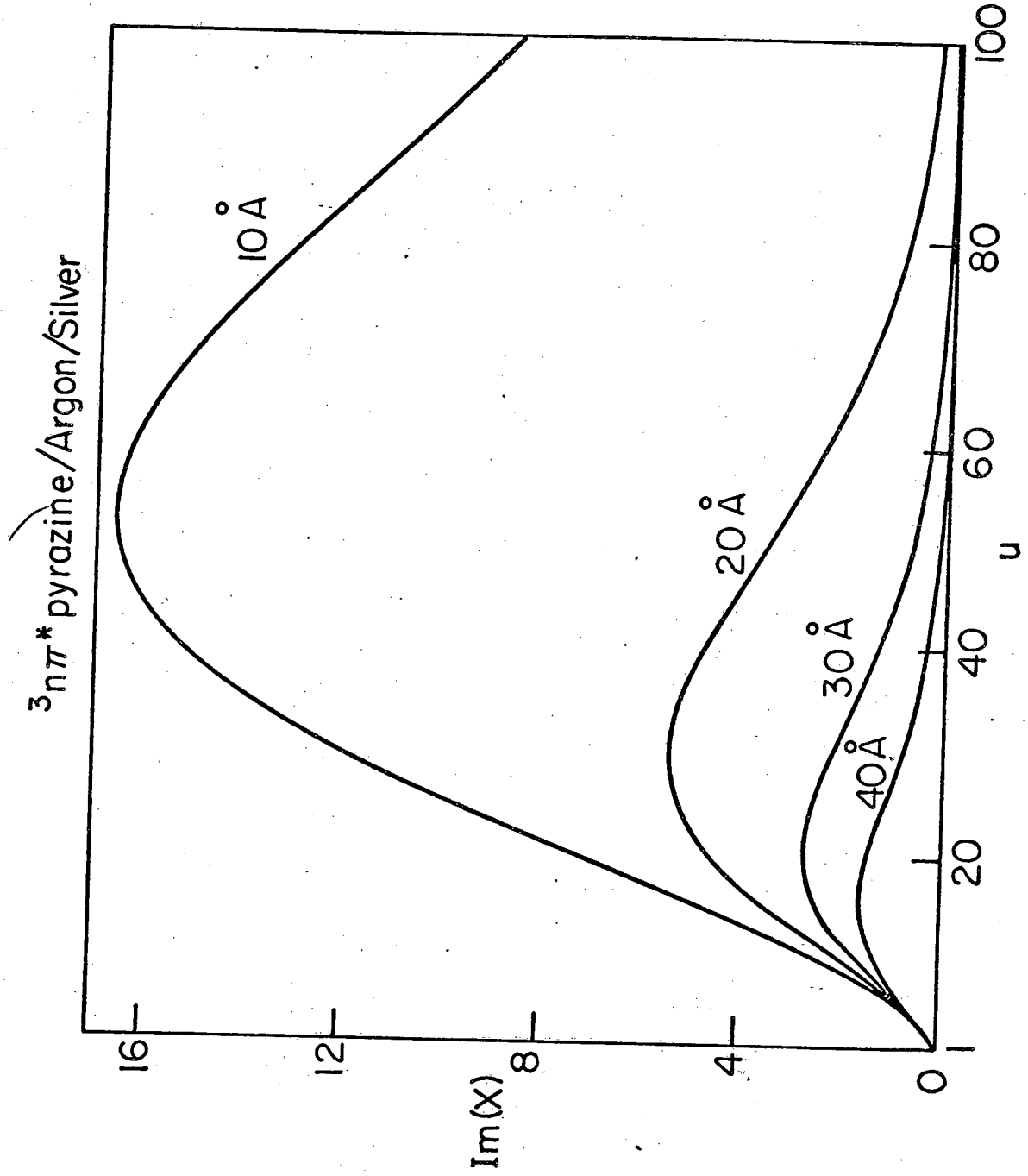
$^3n\pi^*$ pyrazine/Argon/Silver
10 Å
20 Å
30 Å
40 Å
Im(X)
u
0
4
8
12
16
20
40
60
80
100
XBL821-5039

Figure 6b

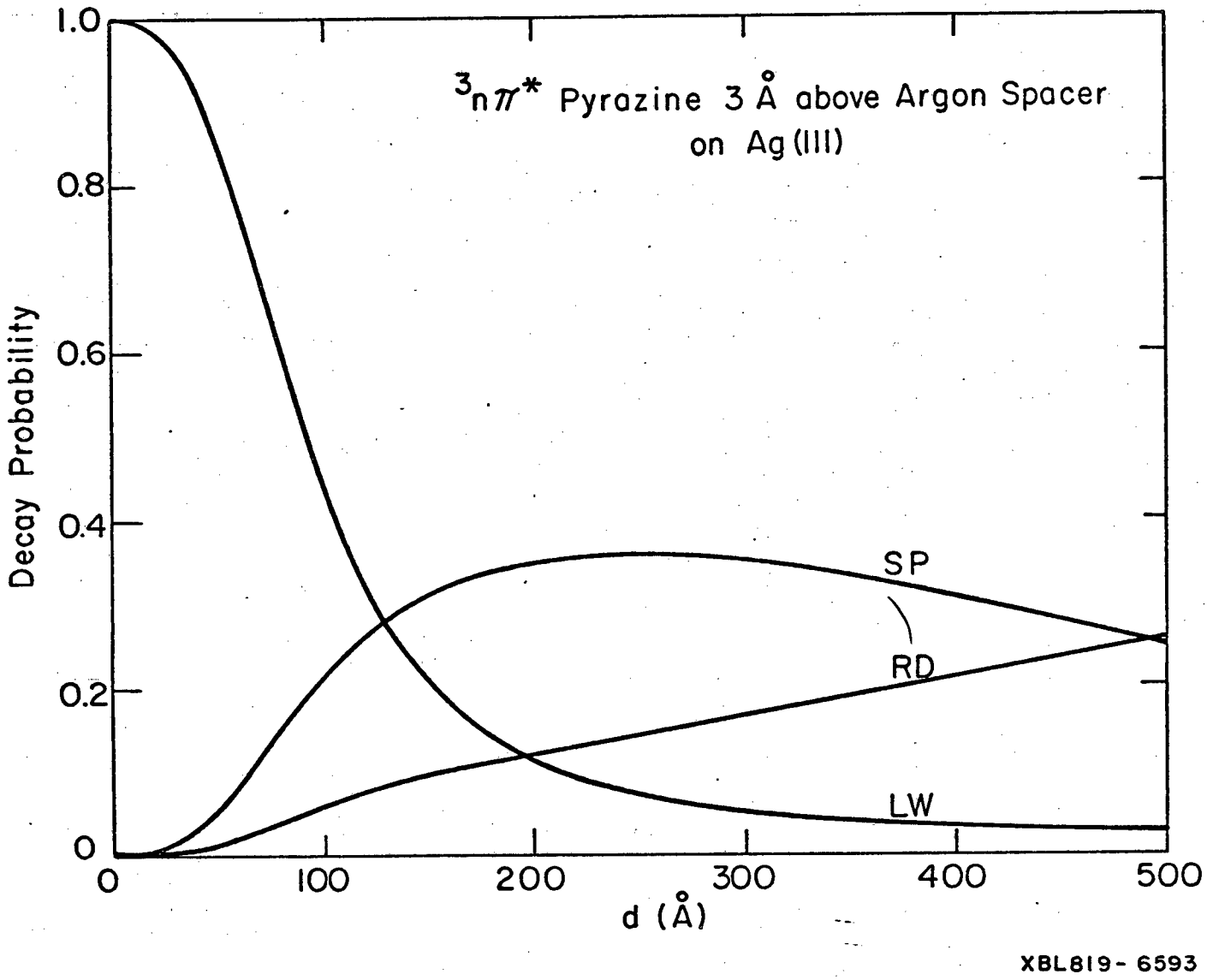
$^3n\pi^*$ Pyrazine 3 Å above Argon Spacer on Ag(111)
Decay Probability
1.0
0.8
0.6
0.4
0.2
0
SP
RD
LW
0
100
200
300
400
500
d (Å)
XBL819-6593

Figure 7

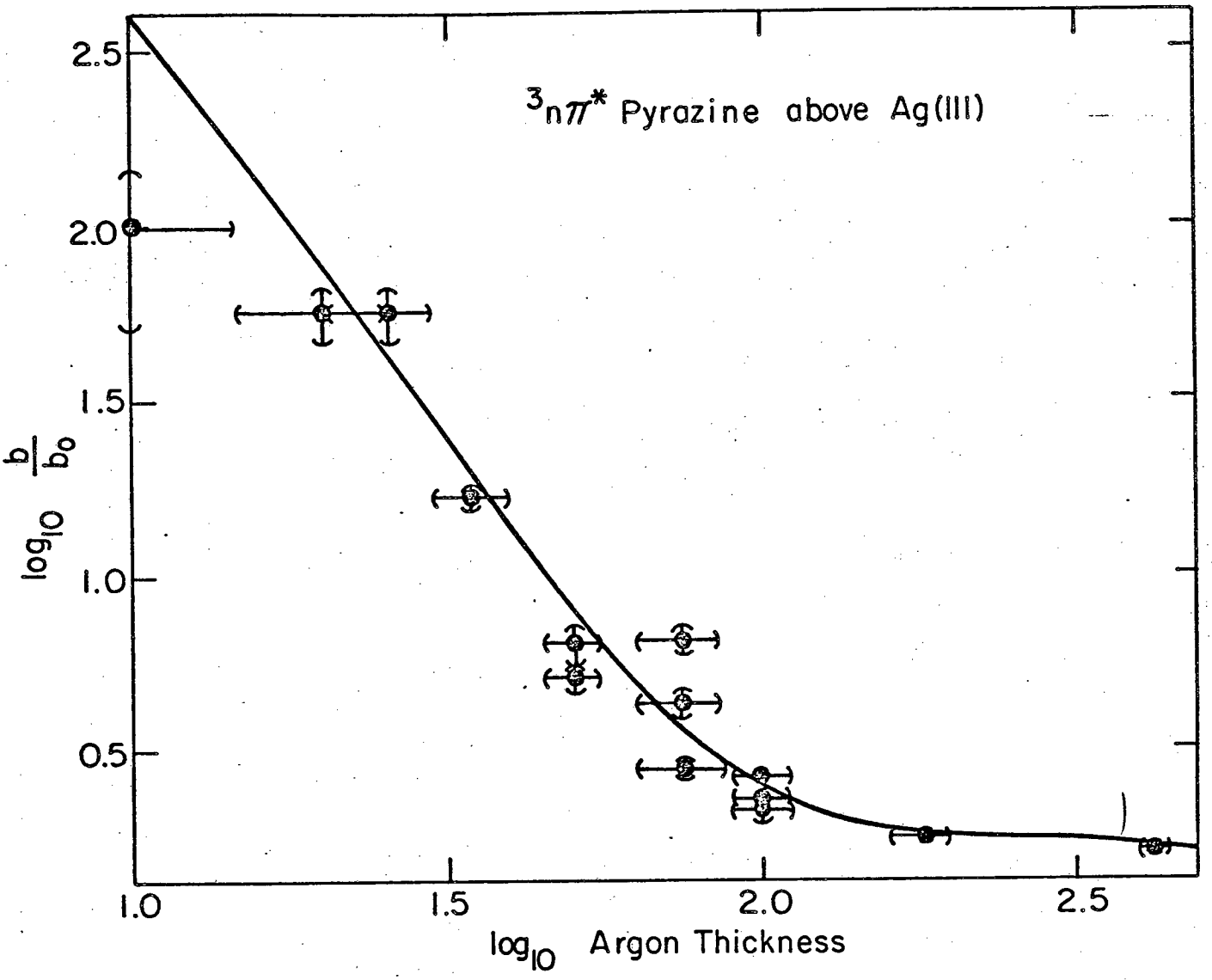
$^3n\pi^*$ Pyrazine above Ag(III)
2.5
2.0
1.5
1.0
0.5
$\log_{10} \frac{b}{b_0}$
1.0
1.5
2.0
2.5
$\log_{10}$ Argon Thickness
XBL 819-6592

Figure 8

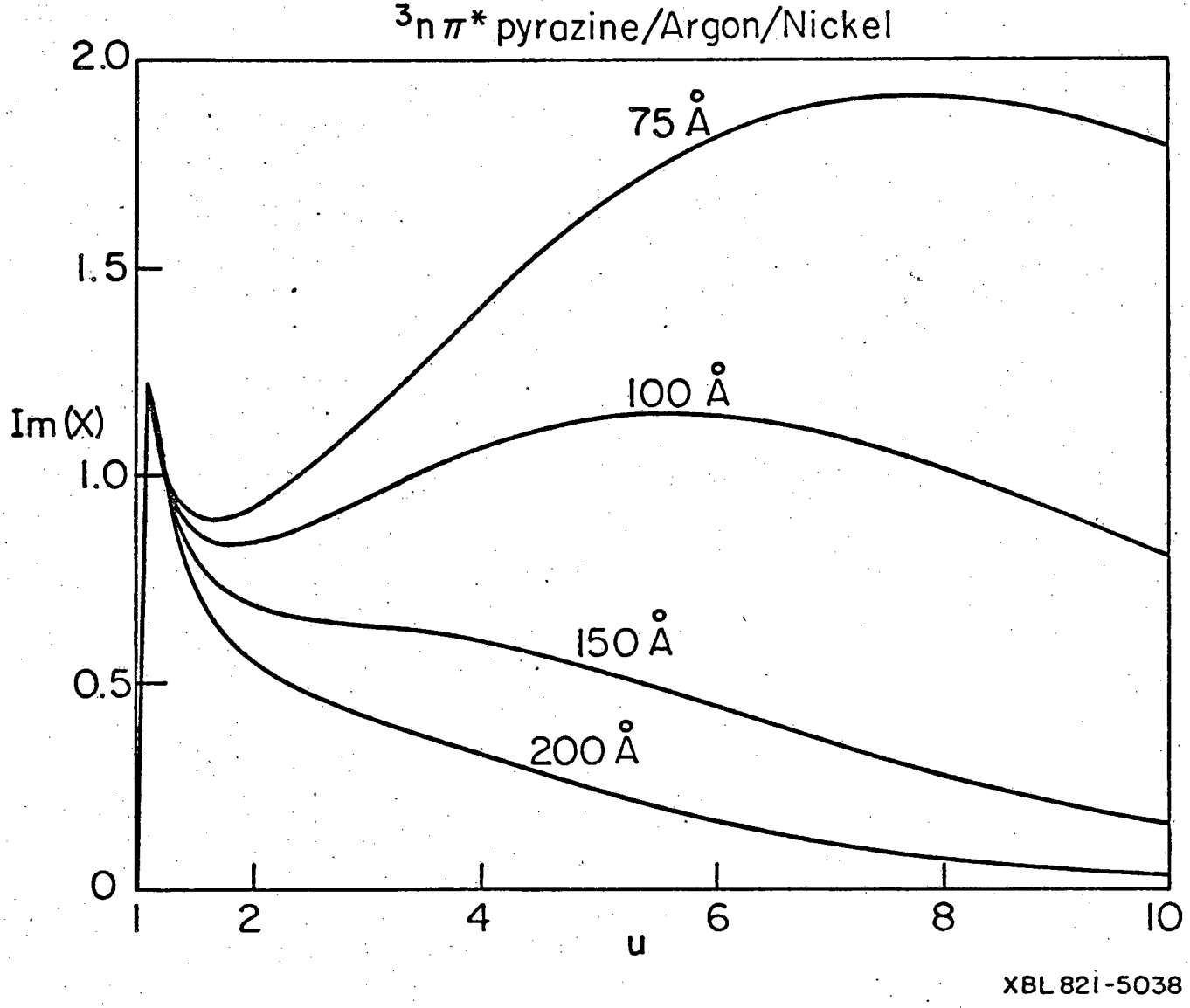
$^3n\pi^*$ pyrazine/Argon/Nickel
2.0
1.5
1.0
0.5
0
Im(X)
75 Å
100 Å
150 Å
200 Å
1
2
4
6
8
10
u
XBL 821-5038

Figure 9a

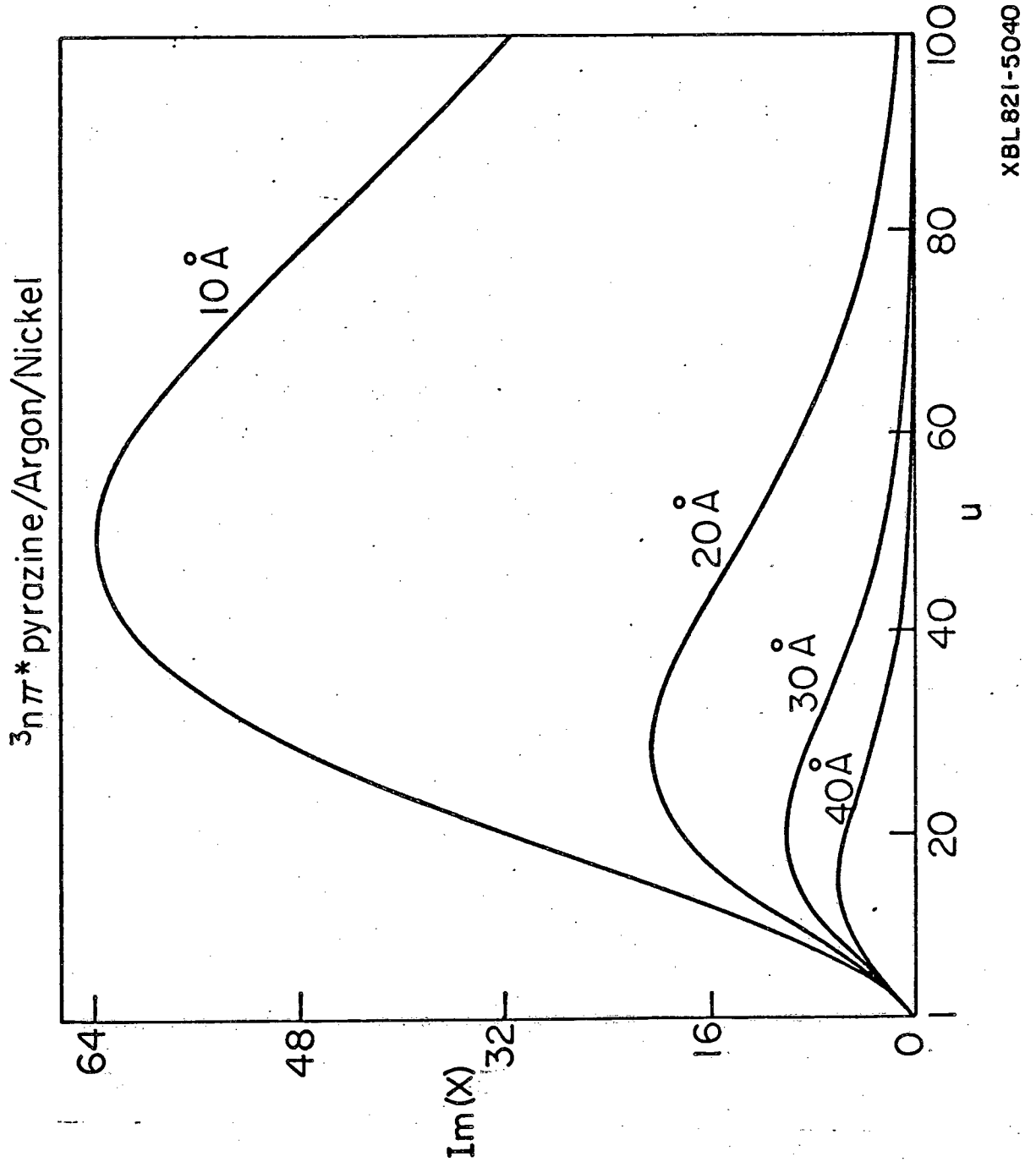
$^3n\pi^*$ pyrazine/Argon/Nickel
10 Å
20 Å
30 Å
40 Å
Im(X)
u
0
16
32
48
64
1
20
40
60
80
100
XBL821-5040

Figure 9b

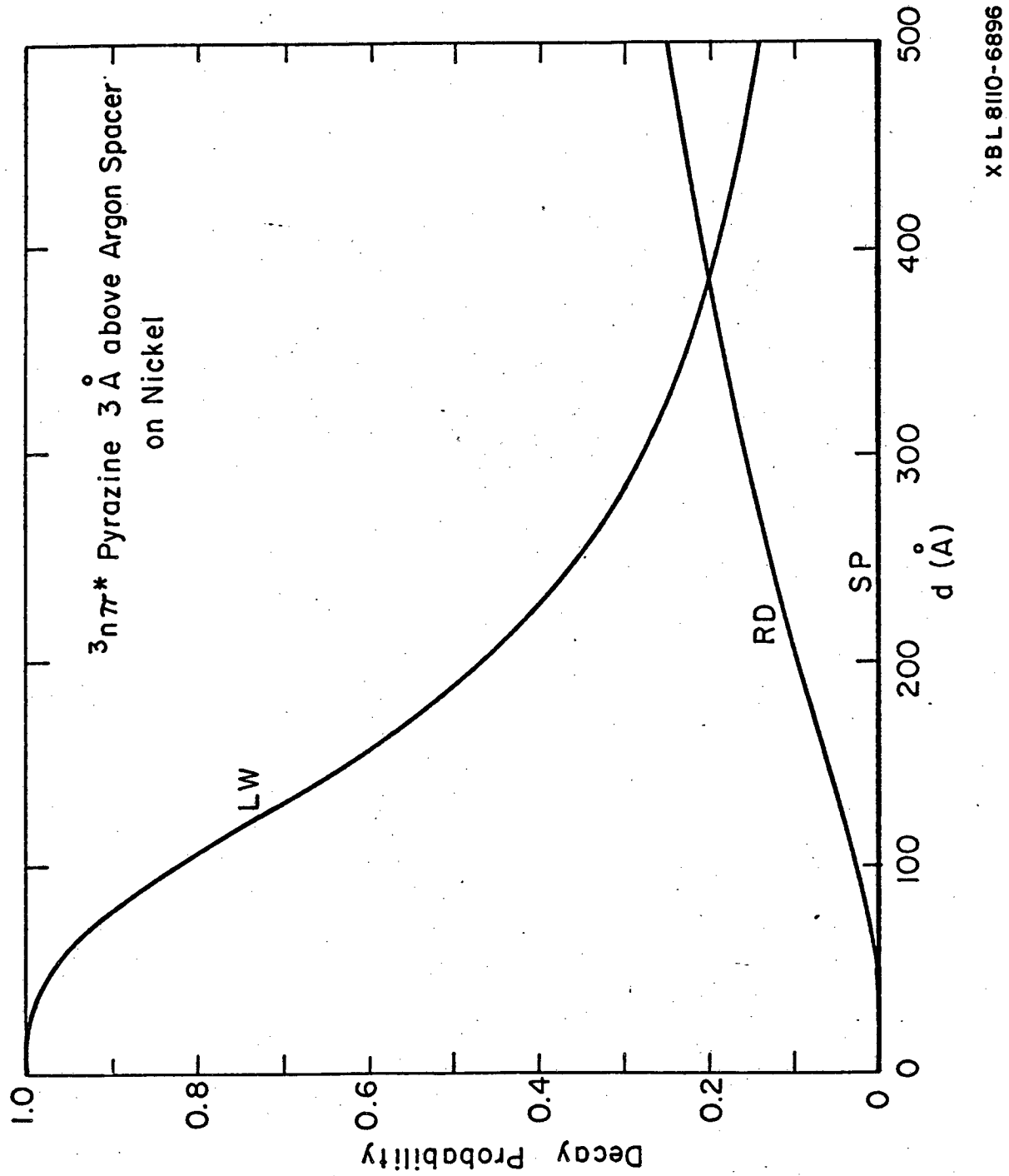
$^3n\pi^*$ Pyrazine 3 Å above Argon Spacer on Nickel
LW
RD
SP
Decay Probability
d (Å)
0
0.2
0.4
0.6
0.8
1.0
100
200
300
400
500
XBL 8110-6896

Figure 10

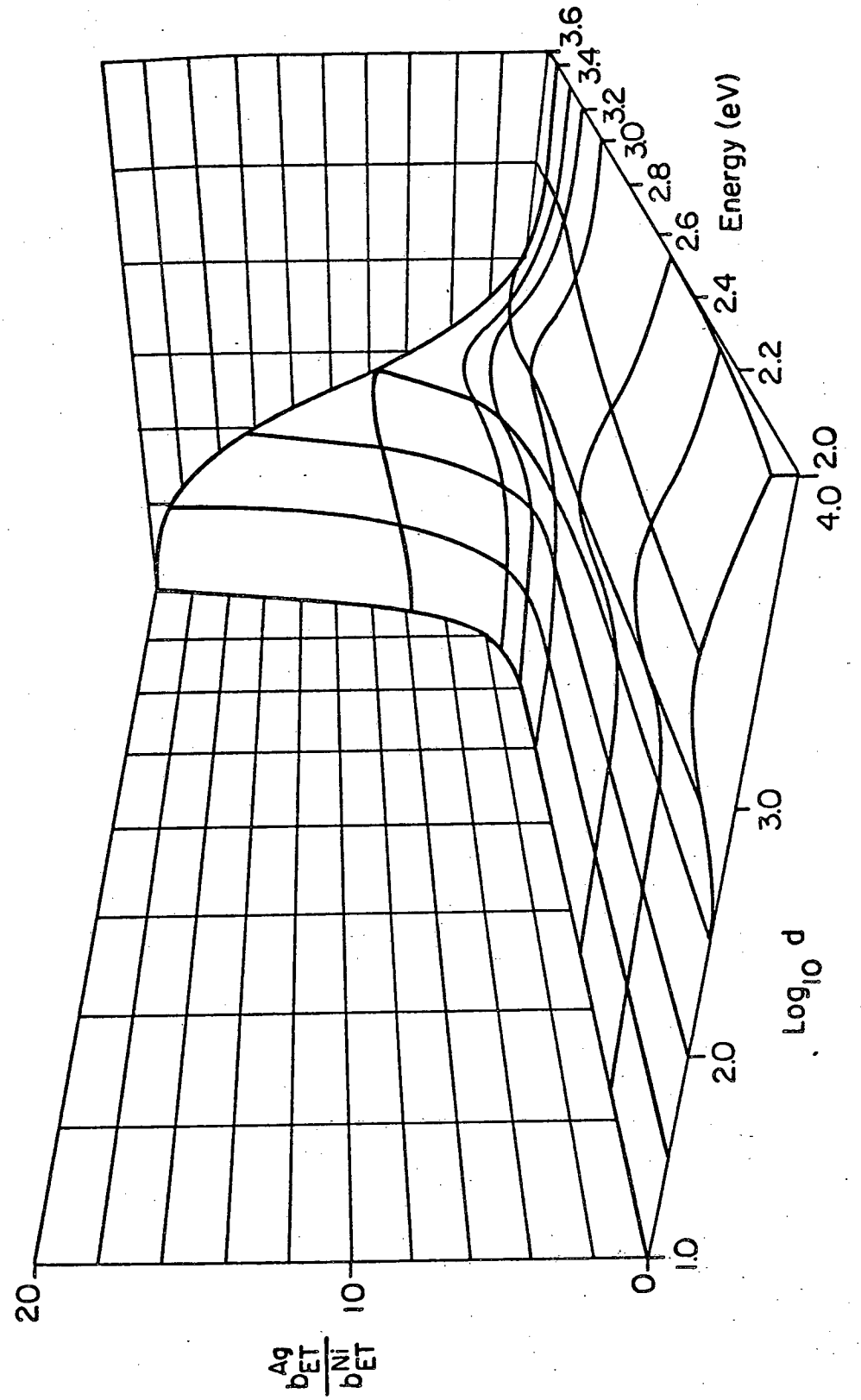

XBL821-5119

Figure 11

This report was done with support from the Department of Energy. Any conclusions or opinions expressed in this report represent solely those of the author(s) and not necessarily those of The Regents of the University of California, the Lawrence Berkeley Laboratory or the Department of Energy.

Reference to a company or product name does not imply approval or recommendation of the product by the University of California or the U.S. Department of Energy to the exclusion of others that may be suitable.

TECHNICAL INFORMATION DEPARTMENT
LAWRENCE BERKELEY LABORATORY
UNIVERSITY OF CALIFORNIA
BERKELEY, CALIFORNIA 94720